Check for updates

Preparation and characterization of hierarchically porous hybrid gels for efficient dye adsorption†

Yong-Kang Xia,‡[a] Xiang-Jun Zha,‡[b] Yu-Xiang She,[a] Ting-Xian Ling,[c] Jing Xiong,[d] Kun-Lan Huang[a] and Ji-Gang Huang ⓘ *[a]

Water treatment faces significant challenges due to the increasing complexity of pollutants and the need for more efficient, sustainable treatment methods. However, current adsorbent materials often struggle with issues such as low adsorption capacity, slow kinetics, and poor reusability, limiting their practical application. In this study, we developed a novel hierarchical porous hybrid gel (HPHG) for water treatment to address the limitations of conventional adsorbents. The HPHG features a multi-level porous structure (from 48 ± 28 nm to 4385 ± 823 nm) that significantly enhances its porosity and specific surface area. We systematically investigated the relationship between the material's structure and its adsorption performance. Kinetic studies revealed a tendency towards a pseudo-second-order adsorption model, attributed to the material's unique structural features that facilitate rapid mass exchange channels inside HPHG and provide abundant active sites for pollutant adsorption. Reusability tests demonstrated that the material retained 85.4% of its initial adsorption capacity after five adsorption–desorption cycles, highlighting its potential for practical applications. This study provides valuable insights into structure–performance relationships in advanced water treatment materials, offering a promising approach for designing next-generation adsorbents with superior efficiency and sustainability.

[a]*School of Mechanical Engineering, Sichuan University, Chengdu, 610065, Sichuan, China. E-mail: jigang.huang@scu.edu.cn*

[b]*Liver Transplant Center, Laboratory of Liver Transplantation, Frontiers Science Center for Disease-Related Molecular Network, West China Hospital of Sichuan University, 610041, Sichuan, China*

[c]*Orthopedic Research Institute & Department of Orthopedics, West China Hospital of Sichuan University, Chengdu, 610041, Sichuan, China*

[d]*Institute of Advance Study, Chengdu University, Chengdu, 610106, Sichuan, China*

† Electronic supplementary information (ESI) available. See DOI: https://doi.org/10.1039/d4ra05844e

‡ Y. Xia and X. Zha contributed equally to this work.

1 Introduction

Water pollution caused by organic dyes has become a significant environmental issue due to their extensive use in industries such as textiles, leather, paper, and plastics.[1–4] These dyes, often toxic and non-biodegradable, pose serious threats to aquatic life and human health. Conventional dye removal methods, including chemical precipitation, membrane filtration, and biological treatment, often fall short in efficiency, cost-effectiveness, and sustainability.[5–11] Consequently, there is an urgent need for innovative materials and methods to effectively address this problem. Recent years have seen the investigation of various materials for dye removal applications.[12–14] Adsorbent materials have garnered significant attention due to their high efficiency and reusability. Activated carbon, with its large surface area and porosity, has long been popular for enhancing adsorption capacity.[15–18] However, its high cost and regeneration difficulties limit practical application. Other materials such as clay minerals, zeolites, and agricultural wastes offer advantages like low cost and availability but often suffer from lower adsorption capacities and selectivity.[19–25] Nanomaterials have emerged as a promising alternative due to their high surface area and unique physicochemical properties.[26–30] For instance, metal–organic frameworks (MOFs) like Zeolitic Imidazolate Framework-8 (ZIF-8) have demonstrated excellent adsorption capacities for various dyes owing to their tunable pore structures and high surface areas.[31–38] However, integrating these nanomaterials into a matrix that facilitates practical application while maintaining or enhancing their adsorption properties remains challenging.

Hydrogels, with their high-water content and tunable properties, have been identified as suitable matrices for incorporating nanomaterials. Composite hydrogels integrating nanoparticles such as ZIF-8 have shown improved dye adsorption capacities due to synergistic effects between the hydrogel matrix and embedded nanomaterials.[39–43] Nonetheless, optimizing these hydrogels' structure to maximize surface area and porosity is crucial for further enhancing their adsorption capacity.

The introduction of multi-level porous structures into nanocomposite hydrogels represents a significant advancement in this field. By creating a hierarchical pore structure, it is

possible to increase the specific surface area and provide more active sites for dye adsorption.[40] In this study, we have developed a multi-level porous nanocomposite hydrogel by incorporating ZIF-8 as a nano-adsorbent and using protein as a foaming agent based on our previous work.[44] The mechanical foaming process generated large pores of approximately 200 micrometers, while the intrinsic hydrogel structure formed smaller pores of about 20 micrometers. Additionally, the ZIF-8 nanoparticles introduced nanometer-scale micropores. We confirmed the successful incorporation of ZIF-8 into the hydrogel matrix through Fourier-transform infrared spectroscopy (FTIR) and X-ray diffraction (XRD). Scanning electron microscopy (SEM) provided evidence of the multi-level porous structure within the hydrogel. We evaluated the performance of this novel hydrogel through adsorption experiments using methylene blue, methyl orange, and rhodamine B as model dyes. The results demonstrated superior dye adsorption capacities compared to traditional hydrogels and nanocomposites. Moreover, the hydrogel exhibited excellent recyclability, maintaining high adsorption efficiency (85.4% for RB) over multiple cycles of dye removal and regeneration.

In summary, this study presents a novel approach to enhancing the performance of nanocomposite hydrogels for dye removal through the introduction of multi-level porous structures. The combination of large, small, and nanometer-scale pores significantly increases the specific surface area and adsorption capacity, offering a promising solution for efficient and sustainable dye removal from wastewater.

1.1 Materials

Soluble lyophilized silk fibroin (SF) was obtained from Simatach Co. Ltd. (Suzhou, China). Acrylamide (AM) (M_n = 71.08), carboxymethyl cellulose (CMC) (M_w = 250 000), and poly(ethylene glycol) diacrylate (PEGDA) (M_n = 600) were purchased from Aladdin Technology Co., Ltd. Lithium phenyl (2,4,6-trimethylbenzoyl) phosphinate (LAP) (photoinitiator) was acquired from EFL Technology Co., Ltd. ZIF-8 nanoparticles (pore size: 0.5–1.1 nm) were sourced from Qiyue Biotechnology Co. Ltd.

1.2 Preparation of foaming printing ink and HPHG

The hierarchically porous hybrid gel (HPHG) was prepared as follows: 0.375 g of CMC and 0.225 g of SF powder were dissolved in 9 mL of AM aqueous solution with varying AM concentrations (10%, 20%, 30% wt%) under low-rate stirring (50 rpm) at 50 °C. Subsequently, 0.03 g of LAP (0.2 wt%) and 0.12 g of PEGDA (0.8 wt%) were incrementally added to the solution under continuous stirring. The solution then underwent unidirectional stirring at 2000 rpm for 15 minutes to form uniformly emulsified foam at room temperature. The foaming precursor was poured into a rectangular mold and exposed to UV irradiation (405 nm) to fabricate HPHG. The resulting HPHG was freeze-dried for dye adsorption applications.

1.3 Characterization

Material morphologies and structures were characterized using a JEOL JSM-5900LV SEM (Tokyo, Japan). Samples were lyophilized and sputter-coated with gold before imaging. FTIR spectroscopy was performed with a Nicolet 560 spectrometer in the range of 600–4000 cm^{-1}. X-ray diffraction analysis was conducted on an Ultima IV X-ray diffractometer (Rigaku, Akishima, Japan) from 2θ angles of 5° to 50° with CuK$_\alpha$ radiation (λ = 0.154056 nm) at a scanning speed of 10° min^{-1}. Dynamic rheological behavior was evaluated using a parallel plate rheometer (TA-AR2000ex, TA Instruments, USA) with a testing frequency range of 0.01 to 100 Hz at 25 °C. Strain sweeps were conducted from 0.01% to 10% at a fixed frequency of 1 Hz to identify the linear viscoelastic region. Rheology samples measured $\varphi2 \times 1$ mm with a 50 μm plate-to-plate distance. Tensile tests were performed at room temperature using an Instron 5967 universal testing machine with a feed speed of 100 mm min^{-1}. Tensile samples measured $60 \times 10 \times 1$ mm.

1.4 Adsorption experiments

Adsorption experiments were conducted using cationic dyes Rhodamine B (RB) and methylene blue (MB), and anionic dye methyl orange (MO). For adsorption kinetics, 500 mg of freeze-dried HPHG was added to 10 mL of 10 mg L^{-1} dye suspension at room temperature under continuous stirring. Aliquots of 3 mL were taken every 30 minutes, and dye concentrations were determined using a UV-visible spectrophotometer. Standard curves for each dye were constructed to facilitate adsorption performance measurements. Adsorption kinetics were studied using pseudo-first-order and pseudo-second-order models. For static adsorption, 500 ± 10 mg of freeze-dried HPHG was added to 10 mL of dye solution (10 mg L^{-1}, pH = 7). For the desorption process, the dyes were removed by washing with ethanol three times, followed by immersion in diluted water for 2 hours. Subsequently, the gel was dried in an oven at 60 °C. Solution concentrations were measured at various time intervals at room temperature (25 °C).

2 Results and discussion

2.1 Design and fabrication of HPHG

The introduction of hierarchically porous structures within hydrogels is an effective strategy to enhance the specific surface area for dye adsorption. In this study, we developed a facile foaming printing strategy for the fabrication of hierarchically porous hybrid hydrogels (HPHG), as illustrated in Fig. 1. To create micropores within the hydrogels, each several hundred microns in size, we devised an environmentally friendly mechanical stirring method incorporating silk fibroin. The inclusion of a thickener ensures uniform and prolonged dispersion of bubbles, enhancing the viscosity and printability of the foaming ink. Following robust magnetic stirring for 10 minutes at 2000 rpm, bubbles are generated and uniformly dispersed in the foaming precursor. This precursor is then exposed to UV irradiation to facilitate cross-linking. The hierarchically porous structures within the hydrogels are designed to offer substantial surface areas, thereby enhancing dye adsorption efficiency. Based on our previous work, we determined that vigorous magnetic stirring at 2000 rpm produces minimal and numerous bubbles that can be effectively
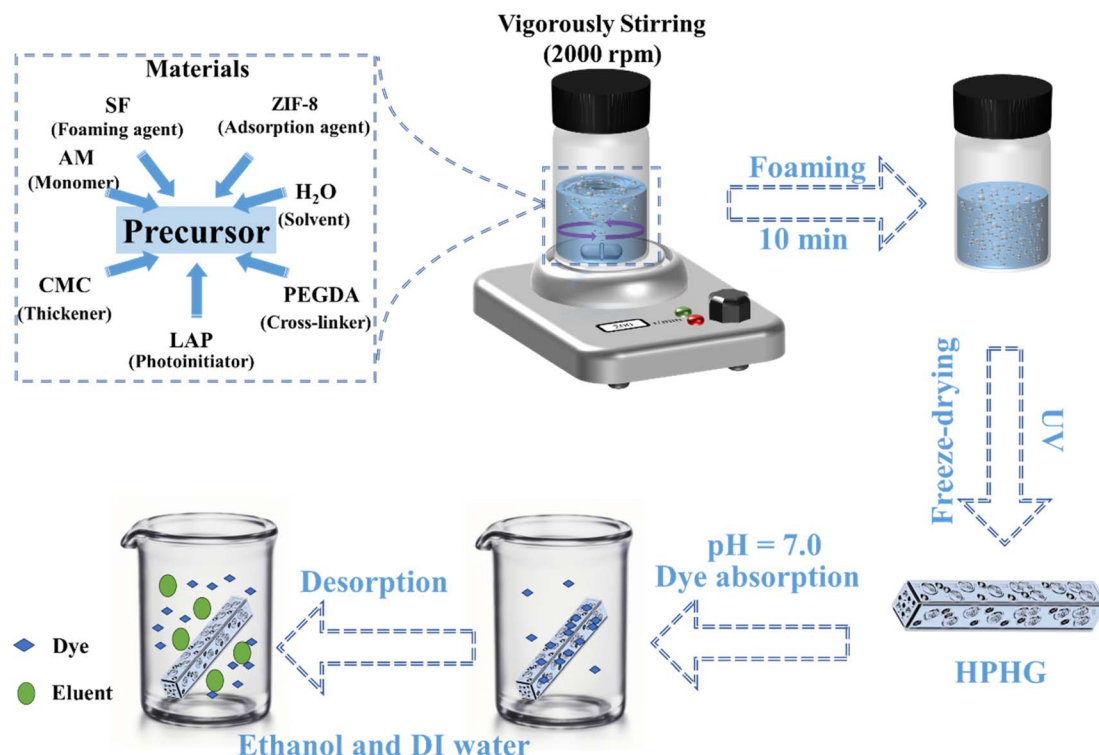
Fig. 1 Schematic illustration of preparation and application of HPHG.

entrapped within gels after UV exposure. Consequently, we selected this stirring rate for the fabrication of HPHG.

2.2 Structural characterization of HPHG

We conducted a detailed investigation into the microstructures of HPHG. Fig. 2A reveals that the intrinsic network of 0ZIF-8 HPHG displayed distinct hierarchically macro-micro-nanoporous structures without the introduction of ZIF-8. The nanopore size of 0ZIF-8 was measured as 48 ± 28 nm, indicating the assembly of silk fibroin (SF), carboxymethyl cellulose (CMC), and ZIF-8. The micropore size, formed by the intrinsic polyacrylamide (PAM) network of ZIF-8 HPHG, remained
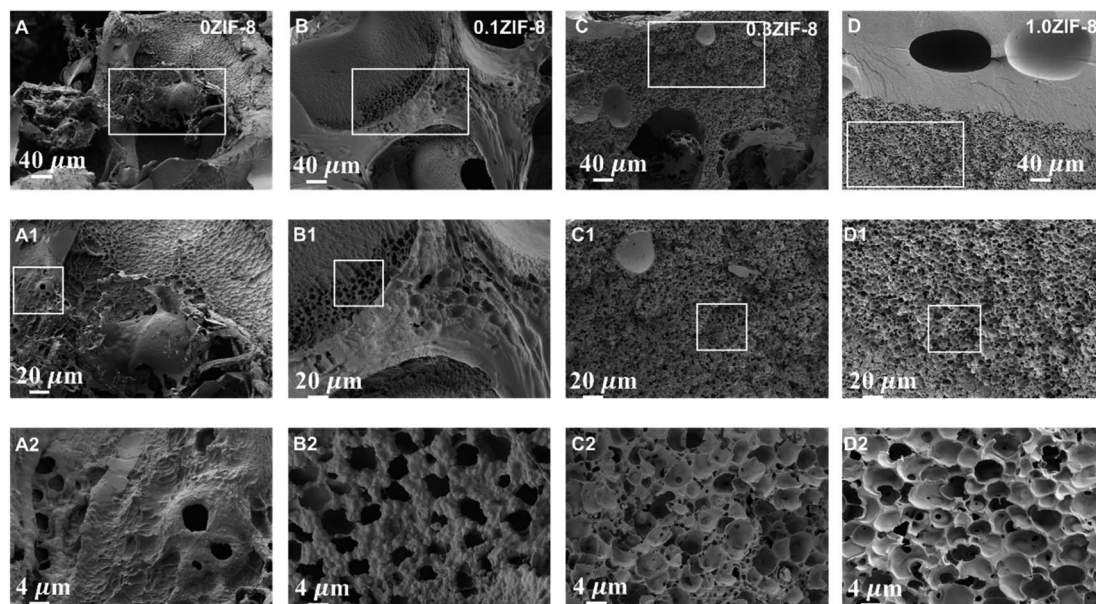

Fig. 2 SEM photos of HPHG with different content of ZIF-8. (A–A2) Images with different magnifications for HPHG without ZIF-8. (B–B2) Images with different magnifications for HPHG with 0.1 wt% ZIF-8. (C–C2) Images with different magnifications for HPHG with 0.3 wt% ZIF-8. (D–D2) Images with different magnifications for HPHG with 1.0 wt% ZIF-8 SEM different magnifications.

consistent across different stirring rates, with a size of 4385 ± 823 nm (Table S1†).

As seen in Fig. 2A, B, S1, and Table S2† the results show that the ZIF-8 has been introduced in HPHG. Fourier-transform infrared spectroscopy (FTIR) was employed to investigate the structural characteristics of hydrogels with different acrylamide (AM) concentrations and stirring rates (Fig. 3C). The spectra reveal distinct adsorption bands at 1530 cm^{-1} (amide II band) and 1630 cm^{-1} (amide I band), indicative of the β-sheets band of SF, suggesting good compatibility between AM and SF and a further reduction in SF crystallinity. As seen in Fig. 3D, major summits at $2\theta = 7.4°$ (011), 10.4° (002), 12.7° (112), 14.8° (022), 16.4° (013), and 18.1° (022) are observed after introduction of ZIF-8, which could be in excellent agreement with the theoretical calculated pattern, suggesting that ZIF-8 has been successfully introduced in HPHG. Fig. 3E and F presents N$_2$ adsorption/desorption and morphological properties of HPHG. Fig. 3F shows the distribution of pores with ∼5.94 nm in pore diameter, implying the major existence of micropores in ZIF-8 structure side HPHG. The Brunauer–Emmett–Teller (BET) theory-calculated totally specific surface area and micropore volume of HPHG were improved from 1.54 m^2 g^{-1} and 4.39 cm^2 g^{-1}, indicating that the introduction of ZIF-8 can improve the surface area of HPHG (Table S3†).

2.3 Rheology behavior of HPHG

In terms of rheological properties, the HPHG exhibited higher storage modulus and loss than those with higher ZIF-8 concentrations (Fig. 4A and B). This suggests that the introduction of ZIF-8 can affect the rheology behavior remarkably.
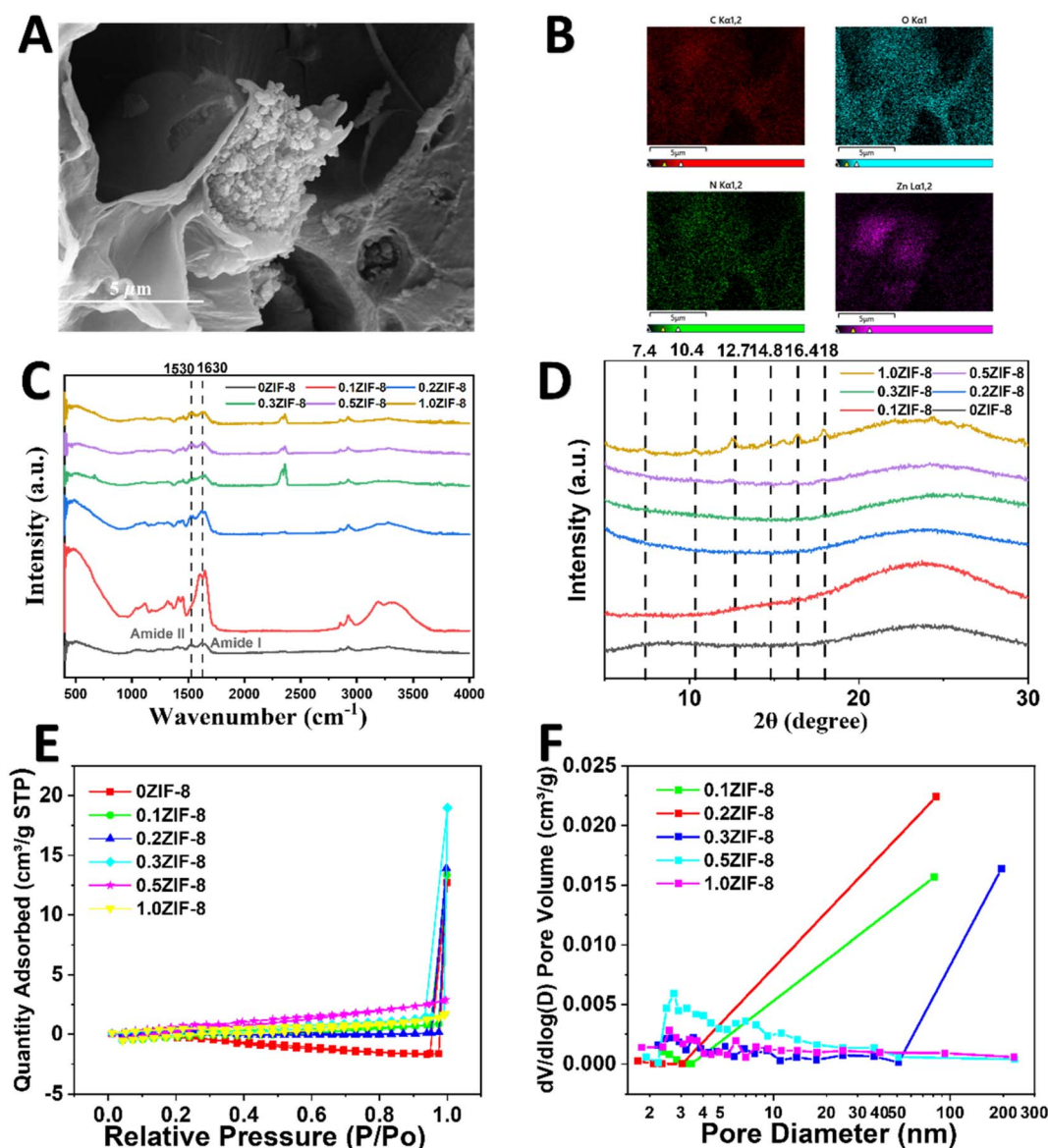

Fig. 3 (A) SEM photo of 0.3ZIF-8. (B) EDS mapping photos of 0.3ZIF-8 with four elements (C, O, N, Zn). (C) FTIR curves of HPHA. (D) XRD curves of HPHA. (E) N$_2$ adsorption–desorption isotherm curves. (F) DFT pore size distribution of HPHG.
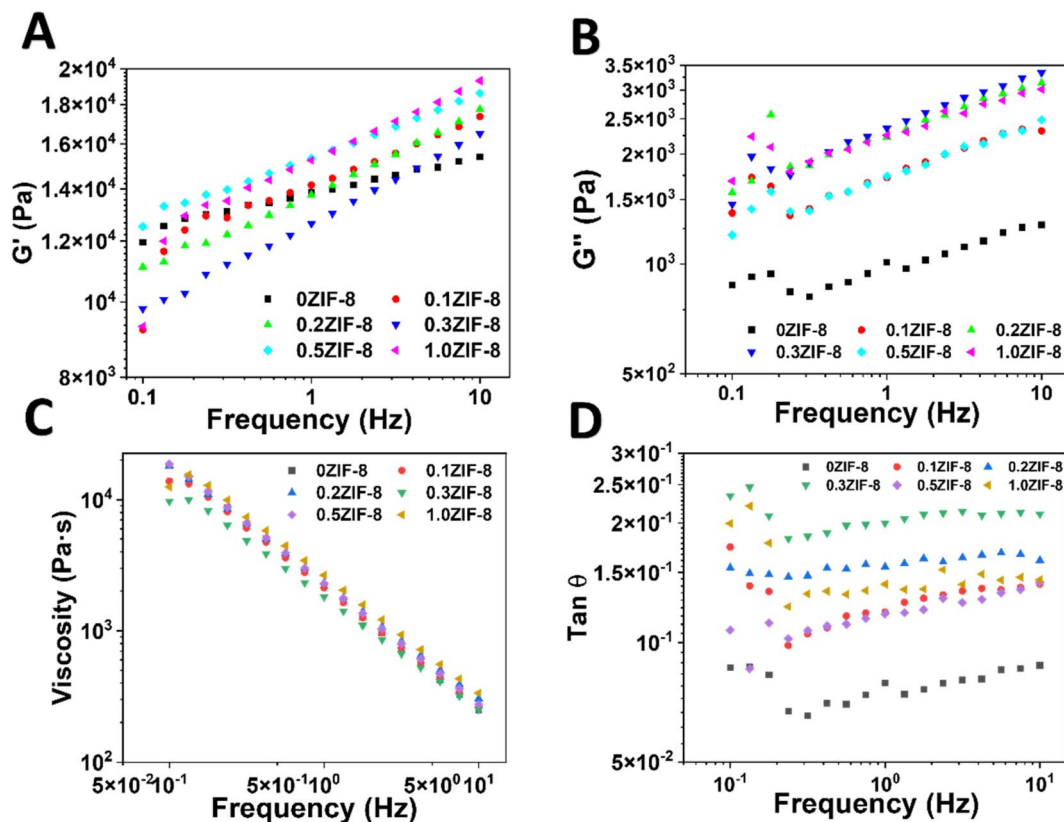
Fig. 4 Oscillatory frequency sweeps of HPHA with different ZIF-8 concentration. (A) Storage modulus, (B) loss modulus, (C) viscosity, and (D) tan θ of HPHG.

However, the introduction of ZIF-8 cannot affect viscosity of HPHG as shown in Fig. 4C. Moreover, all the hydrogels exhibited low tan θ values (<1) (Fig. 4D), indicative of good elasticity across the samples.

2.4 Mechanical property of HPHG

The mechanical properties of various hydrogels were further investigated, leveraging the hierarchically porous structures within HPHG. The HPGH exhibited higher elongation at break after introduction of ZIF-8 (Fig. 5A). The tensile strength, toughness, and moduli of 0.3ZIF-8 HPHG were superior to those of other hydrogels (Fig. 5B and C). The tensile strength of HPHG seems no serious changes in all HPHG. As seen in Fig. 5D and E, the introduction of ZIF-8 has damaged the compressive strength of HPHG, indicating that the ZIF-8 as stress concentration point inside gels.

2.5 Adsorption kinetic characterization of HPHG

Two kinetic models including the pseudo-first-order model, and the pseudo-second-order model were utilized to analyze the detailed adsorption process and mechanism of the freeze-dried HPHG. The concentration of ZIF-8 has been fixed at 0.3 wt% for further investigation. The pseudo-first-order kinetic equation is widely used to analyze the solute with low concentration. It can be represented as the eqn (1).[45]

$$Q_t = Q_e \times (1 - e^{-k_1 t}) \tag{1}$$

where Q_t is the adsorbed dyes amount (mg g^{-1}) at time t, Q_e is the equilibrium adsorption capacity (mg g^{-1}), and k_1 is the rate constant of the equation. As shown in Fig. 6A–D, the plots of absorbance against dyes concentration show a linear relationship. In Fig. 7, the k_1 and Q_e can be obtained from the slope and intercept of the lines. The correlation coefficient values (R^2) of RB and MB adsorption for 0ZIF-8 are 0.964 and 0.968, respectively. The calculated Q_e are 0.155 and 0.175 mg g^{-1}, respectively.

The pseudo-second-order equation is dependent on the surface absorbed amount and the equilibrium absorbed amount.[46] It can be written as follows

$$Q_t = \frac{k_2 Q_e^2 t}{1 + k_2 Q_e t} \tag{2}$$

where k_2 represents the rate constant of the model, Q_t, Q_e and t are the same as those in eqn (1). Fig. 6F and H exhibits the plots of Q_t versus t. The k_2 and equilibrium adsorbed amount (Q_e) can be obtained from the intercept and the slope of the plot lines. As shown in Fig. 8, R^2 of RB and MB adsorption 0ZIF-8 are all higher than 0.9 and the calculated data of Q_e are closer to the experimental values, indicating that the adsorption process agrees well with the pseudo-second-order model.
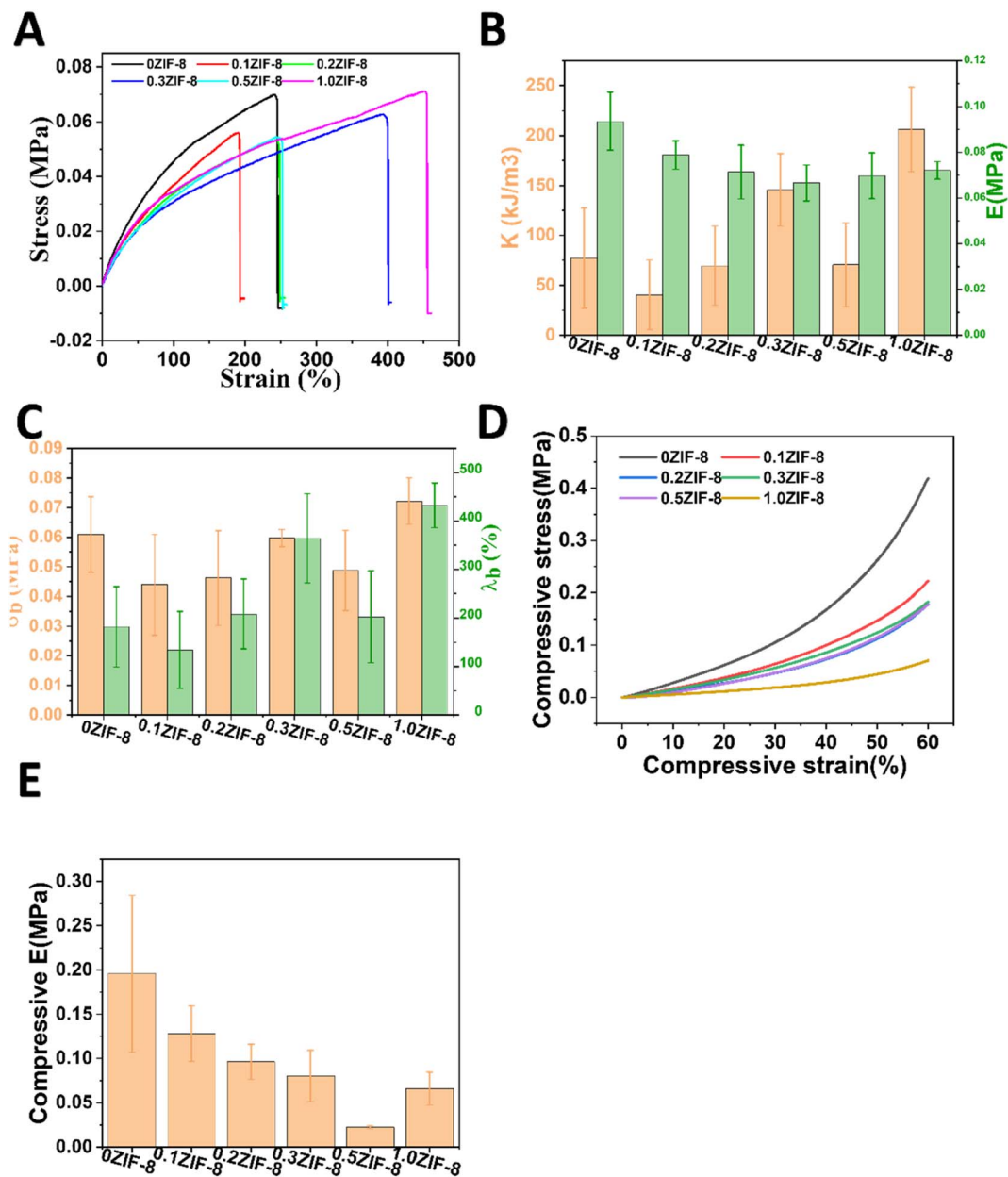
Fig. 5 (A) Typical tensile curves of HPHG. (B) Tensile strength (σ_b) and elongation at break (λ_b) of HPHA. (C) Toughness (K), (D) fracture energy (Γ) of HPHG, and (E) compressive moduli.

Adsorption isotherms can be used to describe the adsorption property and equilibrium data. In order to optimally design the adsorption process, it is essential to establish the most appropriate correlation for the equilibrium curve. In this study, Langmuir and Freundlich adsorption isotherms were utilized to investigate the adsorption process. The Langmuir adsorption isotherm is one of the most commonly used models to investigate the adsorption equilibrium, which supposes that adsorption of dyes occurs on a homogenous surface through monolayer adsorption.[47] The Langmuir formula is written as follows:

$$Q_e = (K_L \times Q_m \times m \times C_e)/(1 + K_L \times C_e) \qquad (3)$$

where K_L represents the Langmuir adsorption constant, C_e is the equilibrium concentration of the dyes (mg L^{-1}), Q_e is the same meaning as that in eqn (1), and Q_m represents the maximum adsorbed amount of the HPHG (mg g^{-1}). As shown in Fig. 6I and K, the plots of Q_e versus C_e yield straight lines. For the optimization of the concentration of the ZIF-8 particles, we also investigated the dye adsorption capability of HPGH with different concentration of ZIF-8 (Fig. S4†). And the values of Q_m and K_L can be calculated from the slopes and intercepts of the obtained straight lines for further investigation (Fig. S5†). Both the R^2 for the Langmuir model are higher than 0.95, which indicates that the adsorption process of the 0ZIF-8 and 0.3ZIF-8 fits well with the Langmuir adsorption isotherm. It can be also
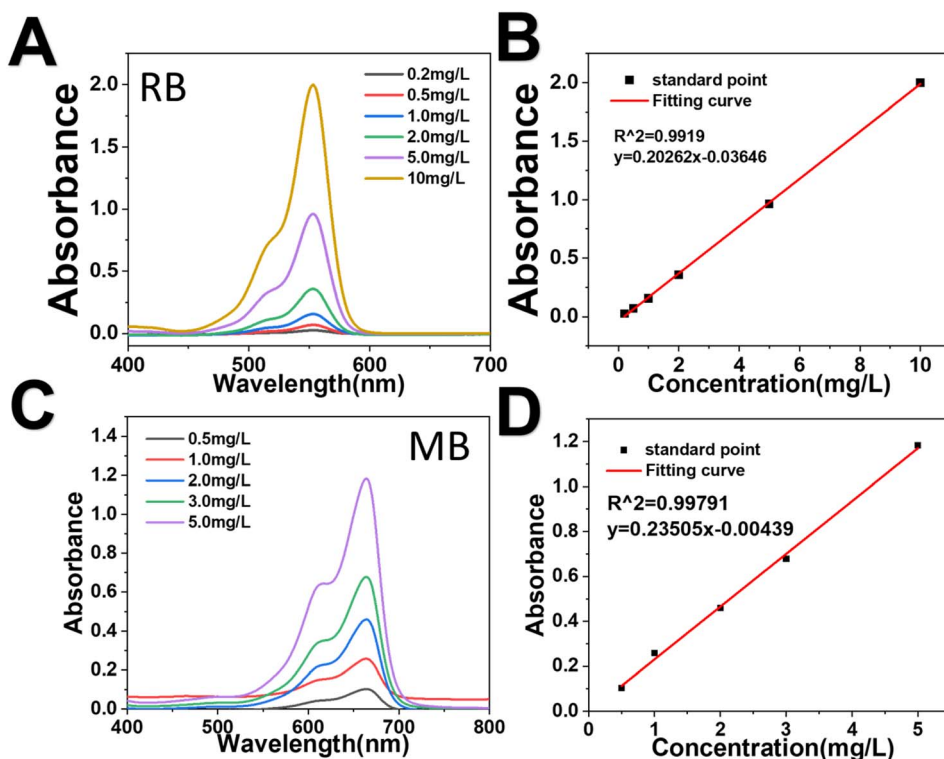
Fig. 6 Adsorption kinetics of RB and MB adsorbed by HPHG. (A and B) Standard concentration curve of RB. (C and D) Standard concentration curve of MB.
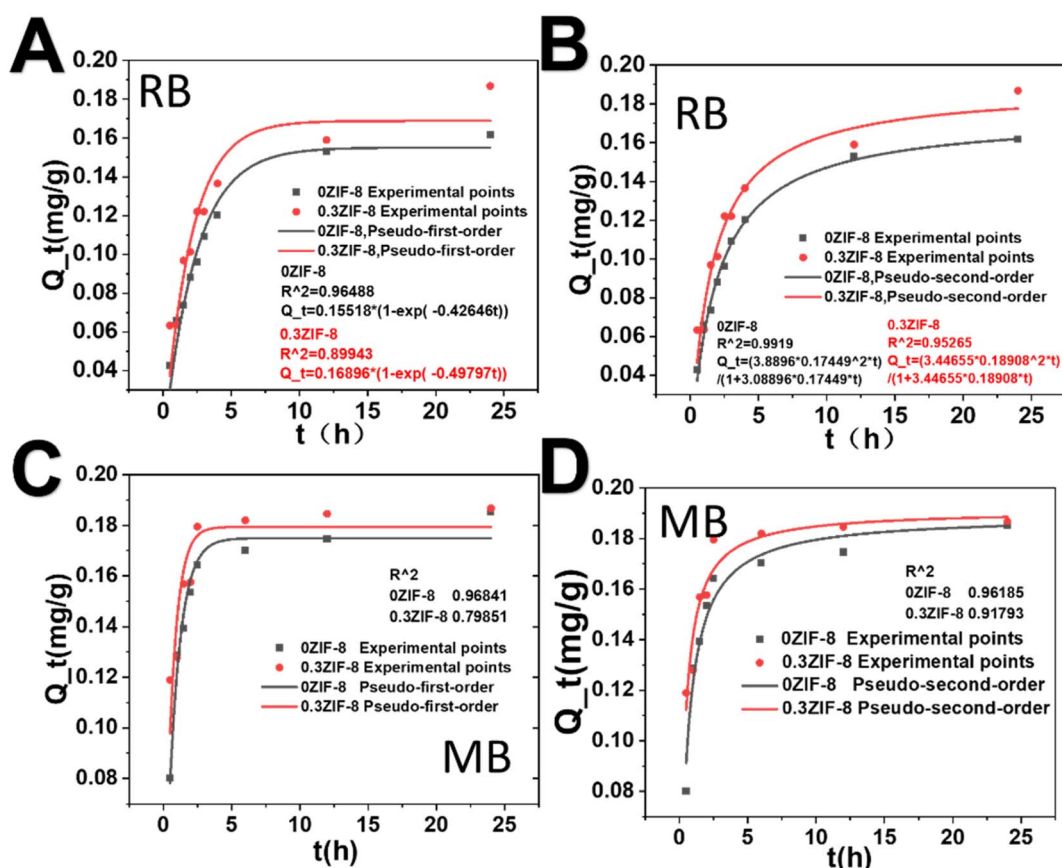

Fig. 7 (A) Pseudo-first-order adsorption model and (B) pseudo-second-order adsorption model for the adsorption of RB by HPHG. (C) Langmuir adsorption isotherm and (D) Freundlich adsorption isotherm of RB onto HPHG.
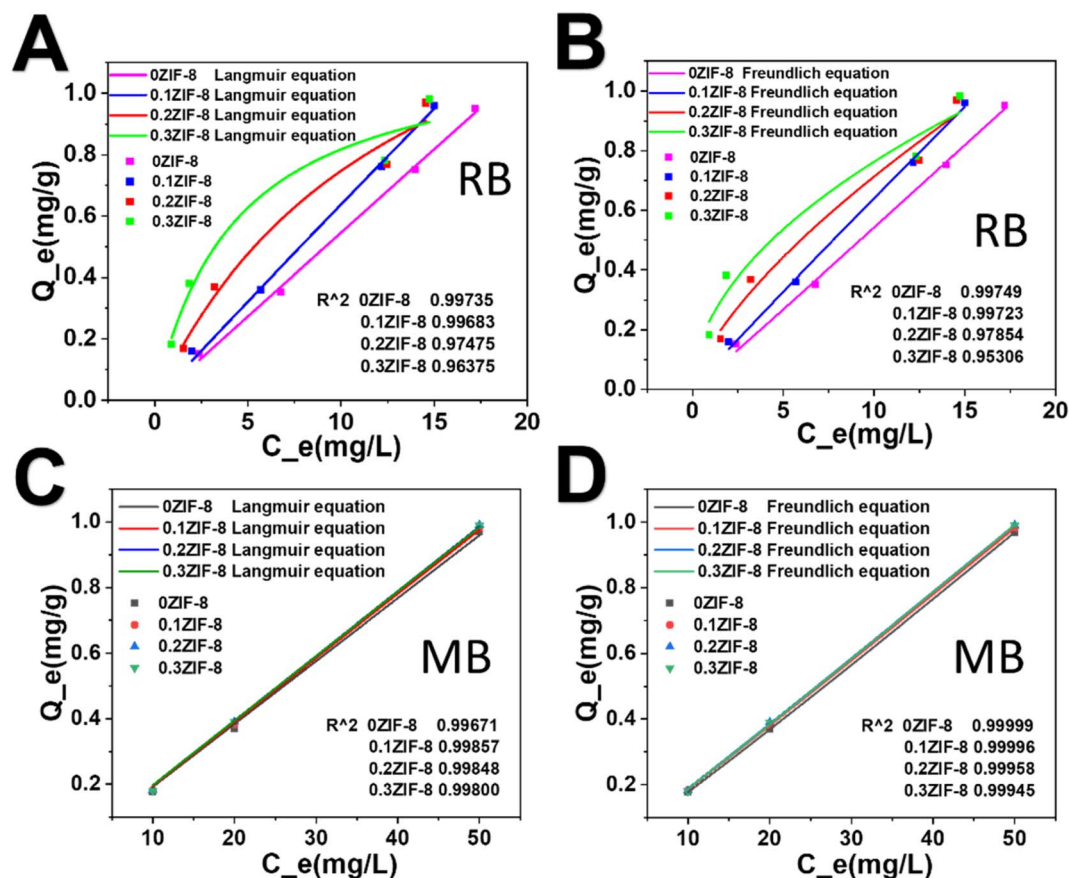
Fig. 8 (A) Pseudo-first-order adsorption model (B) pseudo-second-order adsorption model for the adsorption of MB by HPHG. Pseudo-second-order adsorption model for the adsorption of MB by HPHG. (C) Langmuir adsorption isotherm and (D) Freundlich adsorption isotherm of MB onto HPHG.

found that the 0.3ZIF-8 gel presents higher calculated adsorption capacity and equilibrium adsorbed amount than those of the 0-ZIF-8 gel, indicating that the introduction of ZIF-8 could improve the adsorbability of RB. The Freundlich isotherm[4] is usually written as:

$$Q_e = K_F \times C_e^{1/n} \qquad (4)$$

where K_F is Freundlich isotherm constant, $1/n$ the influence coefficient of solution concentration to the equilibrium adsorption capacity, and Q_e and C_e are the same as those in eqn (3). k_F and n can be obtained from the intercepts and slopes of the fitted lines plotted by Q_e against C_e (Fig. 6J and L). The linear correlation coefficient of 0.3ZIF-8 is higher than 0.96, which is similar than that for the Langmuir model. Meanwhile, the correlation coefficient (0.94) of GOSF20 is smaller than that (0.97) for the Langmuir model. The values of n at the equilibrium (1.97 for RB and 0.97 for MB, respectively) are higher than 1, indicating the excellent adsorption of RB than MB for those prepared 0.3ZIF-8 gel. As shown in Fig. S2 and S3†, the color of dye solution is shallow and the color of the samples are dark, also indicating such results. Furthermore, we also investigated cyclic adsorption ability of 0.3ZIF-8 gel for RB, and MB. The results show a good cyclic adsorption of 0.3ZIF-8 gel for RB and

MB (67.5% and 85.4% after five cycles, respectively). The HPHG demonstrates excellent reusability, attributed to the specific hierarchically porous structures and numerous functional groups—such as carboxyl and amide groups of silk fibroin. These functional groups serve as effective physical adsorption sites, enabling successful adsorption and desorption even after five cycles. In addition, MO dye adsorption effect of HPHG. The HPHG exhibits low adsorption ability for MO. It may be related to the negative zeta potential of HPHG as shown in Fig. S6 and S7.†

3 Conclusion

In this study, we proposed a universe strategy to fabricate multi-level hierarchically porous nanocomposite hydrogels with excellent balance of mechanical, adsorption, and reusable property. Kinetic studies revealed a tendency towards a pseudo-second-order adsorption model, attributed to the material's unique structural features that facilitate rapid mass exchange channels inside HPHG and provide abundant active sites for pollutant adsorption. Reusability tests demonstrated that the material retained 85.4% of its initial adsorption capacity after five adsorption–desorption cycles, highlighting its potential for practical applications. The excellent reusability of HPHG

further confirms that physical adsorption is the primary mechanism governing its adsorption capabilities. This study paves new road in structure–performance relationships in advanced water treatment materials, offering a promising approach for designing next-generation adsorbents with superior efficiency and sustainability.

Data availability

The data supporting this article have been included as part of the ESI.†

Conflicts of interest

The authors declare that they have no competing interests.

Acknowledgements

References

1 Y. Li, M. Wang, J. Liu, L. Han, Q. Qin and X. Liu, Adsorption/desorption behavior of ionic dyes on sintered bone char, *Mater. Chem. Phys.*, 2023, **297**, 127405.

2 P. K. Singh, K.-Y. Kuo, J.-T. Lee, P.-H. Hsiao, J. C. Juan, H. P. Duong and C.-Y. Chen, Synergistic absorbents based on SnFe$_2$O$_4$@ZnO nanoparticles decorated with reduced graphene oxide for highly efficient dye adsorption at room temperature, *RSC Adv.*, 2021, **11**, 17840–17848.

3 D. Liu, J. Wang, X. Liu and D. Shu, Eco-friendly sustainable adsorption dyeing of MOF-modified carboxymethyl cellulose fiber fabric using acid dyes, *Cellulose*, 2024, 1–22.

4 S. Wang, H. Ning, N. Hu, K. Huang, S. Weng, X. Wu, L. Wu, J. Liu and Alamusi, Preparation and characterization of graphene oxide/silk fibroin hybrid aerogel for dye and heavy metal adsorption, *Composites, Part B*, 2019, **163**, 716–722.

5 B. Luan Tran, H.-Y. Chin, B. K. Chang and A. S. T. Chiang, Dye adsorption in ZIF-8: The importance of external surface area, *Microporous Mesoporous Mater.*, 2019, **277**, 149–153.

6 Z. Ma, C. Liu, C. Srinivasakannan, L. Li and Y. Wang, Synthesis of magnetic Fe$_3$O$_4$-HKUST-1 nanocomposites for azo dye adsorption, *Arab. J. Chem.*, 2023, **16**, 104767.

7 F. Shafiq, C. Liu, H. Zhou, H. Chen, S. Yu and W. Qiao, Adsorption mechanism and synthesis of adjustable hollow hydroxyapatite spheres for efficient wastewater cationic dyes adsorption, *Colloids Surf., A*, 2023, **672**, 131713.

8 M. Kert and J. Skoko, Formation of pH-responsive cotton by the adsorption of methyl orange dye, *Polymers*, 2023, **15**, 1783.

9 M. Jiang, R. Simayi, A. Sawut, J. Wang, T. Wu and X. Gong, Modified β-Cyclodextrin hydrogel for selective adsorption and desorption for cationic dyes, *Colloids Surf., A*, 2023, **661**, 130912.

10 Q. Huang, Y. Zhou, Z. Fu and J. Zhu, Preparation of an injectable hydrogel reinforced by graphene oxide and its application in dye wastewater treatment, *J. Mater. Sci.*, 2023, **58**, 3117–3133.

11 S. Peter, N. Lyczko, D. Gopakumar, H. J. Maria, A. Nzihou and S. Thomas, Nanocellulose and its derivative materials for energy and environmental applications, *J. Mater. Sci.*, 2022, **57**, 6835–6880.

12 K.-D. Zhang, F.-C. Tsai, N. Ma, Y. Xia, H.-L. Liu, X.-Q. Zhan, X.-Y. Yu, X.-Z. Zeng, T. Jiang, D. Shi and C.-J. Chang, Adsorption behavior of high stable Zr-based MOFs for the removal of acid organic dye from water, *Materials*, 2017, **10**, 205.

13 Q. Li, H. Li, X. Zong, H. Sun, Y. Liu, Z. Zhan, S. Mei, Y. Qi, Y. Huang and Y. Ye, Highly efficient adsorption of ciprofloxacin from aqueous solutions by waste cation exchange resin-based activated carbons: Performance, mechanism, and theoretical calculation, *Sci. Total Environ.*, 2024, **912**, 169534.

14 Q. Li, Y. Ye, W. Li, F. Pan, D. Xia and A. Li, The efficient adsorption of tetracycline from aqueous solutions onto polymers with different N-vinylpyrrolidone contents: equilibrium, kinetic and dynamic adsorption, *Environ. Sci. Pollut. Res.*, 2023, **30**, 15158–15169.

15 A. A. El Ashmawy, M. Tada and C. Yoshimura, Weak dehydration enhances the adsorption capacity of boehmite for anionic dyes, *Colloids Surf., A*, 2023, **674**, 131954.

16 L. Wang, Y. Yu, H. Hu, B. Xie, Y. Du and Q. Zhu, Quaternized hollow TiO$_2$-enhanced the dye adsorption capacity and photogenerated carrier separation for efficient reactive dye removal, *Appl. Surf. Sci.*, 2024, **644**, 158764.

17 M. Saghian, S. Dehghanpour and M. Sharbatdaran, Unique and efficient adsorbents for highly selective and reverse adsorption and separation of dyes *via* the introduction of SO$_3$H functional groups into a metal–organic framework, *RSC Adv.*, 2020, **10**, 9369–9377.

18 Q. Li, F. Pan, W. Li, D. Li, H. Xu, D. Xia and A. Li, Enhanced adsorption of bisphenol A from aqueous solution with 2-vinylpyridine functionalized magnetic nanoparticles, *Polymers*, 2018, **10**, 1136.

19 M. Rehan, H. El-Sayed, N. S. El-Hawary, H. Mashaly and N. S. Elshemy, Concurrent Dyeing and Finishing of Textile Fabrics Using Chemically Modified Peanut Red Skin Extract, *Ind. Eng. Chem. Res.*, 2024, **63**, 11301–11319.

20 L. R. Oviedo, V. R. Oviedo, L. D. Dalla Nora and W. L. da Silva, Adsorption of organic dyes onto nanozeolites: A machine learning study, *Sep. Purif. Technol.*, 2023, **315**, 123712.

21 J. Miao, L. Xing, J. Ouyang, Z. Li and X. Wang, Adsorption properties of anionic dyes on quaternized microcrystalline cellulose, *ACS Omega*, 2023, **8**, 5617–5624.

22 L. Khezami, A. Bessadok, M. Ali Ben Aissa, A. H. Ahmed, A. Modwi, N. Benhamadi and A. Amine Assadi, Revolutionizing dye removal: g-C$_3$N$_4$-Modified ZnO nanocomposite for exceptional adsorption of basic fuchsin dye, *Inorg. Chem. Commun.*, 2024, **164**, 112413.

23 M. Fayazi and E. Rezvannejad, Bio-inspired preparation of silver nanoparticles on nanostructured sepiolite clay: Characterization and application as an effective adsorbent for methylene blue removal, *Inorg. Chem. Commun.*, 2024, **159**, 111786.

24 M. Fayazi, D. Afzali, M. Taher, A. Mostafavi and V. Gupta, Removal of Safranin dye from aqueous solution using magnetic mesoporous clay: Optimization study, *J. Mol. Liq.*, 2015, **212**, 675–685.

25 M. Fayazi, M. Ghanei-Motlagh and M. A. Taher, The adsorption of basic dye (Alizarin red S) from aqueous solution onto activated carbon/γ-Fe$_2$O$_3$ nano-composite: kinetic and equilibrium studies, *Mater. Sci. Semicond. Process.*, 2015, **40**, 35–43.

26 F. J. Cano, O. Reyes-Vallejo, A. Ashok, M. d. l. L. Olvera, S. Velumani and A. Kassiba, Mechanisms of dyes adsorption on titanium oxide–graphene oxide nanocomposites, *Ceram. Int.*, 2023, **49**, 21185–21205.

27 S. Bokka, P. Ameta, A. K. Lakshya and A. Chowdhury, Remarkable dye adsorption capabilities in CaO-Doped-Zirconia systems, *Appl. Surf. Sci.*, 2024, **659**, 159914.

28 G. Jethave, U. Fegade, S. Attarde, S. Ansar, C. Bathula, S. Kolate and R.-J. Wu, Adsorption of Fuchsine Dye on TiZnPbO Nanocomposites: Analytical Modeling and Interpretation, *ChemistrySelect*, 2023, **8**, e202300678.

29 A. Samy, A. M. Ismail and H. Ali, Environmentally friendly mesoporous SiO$_2$ with mixed fiber/particle morphology and large surface area for enhanced dye adsorption, *J. Mater. Sci.*, 2023, **58**, 1586–1607.

30 Z. Zhang, R. Shi, F. Wang, S. Wang, G. Fu, X. Zou, L. Li, L. Yu, Y. Tian and F. Luo, Separable magnetic MoS$_2$@Fe$_3$O$_4$ nanocomposites with multi-exposed active edge facets toward enhanced adsorption and catalytic activities, *J. Mater. Sci.*, 2021, **56**, 5015–5030.

31 M. Mahreni, R. R. Ramadhan, M. F. Pramadhana, A. P. Permatasari, D. Kurniawati and H. S. Kusuma, Synthesis of metal organic framework (MOF) based Ca-Alginate for adsorption of malachite green dye, *Polym. Bull.*, 2022, **79**, 11301–11315.

32 Q. Wang, X. Zhang, F. Wang, Y. Xie, C. Wang, J. Zhao, Q. Yang and Z. Chen, Egg yolk/ZIF-8/CLPAA composite aerogel: Preparation, characterization and adsorption properties for organic dyes, *J. Solid State Chem.*, 2021, **299**, 122158.

33 H. Jiang, M. Xu, C. Leng, Q. Ma, J. Dai, S. Feng, N. Wang, J. Wei and L. Wang, Bifunctional MOF-5@ coal-based fiber membrane for oil-water separation and dye adsorption, *Colloids Surf., A*, 2024, **683**, 133021.

34 S. Chang, Y. Simeng, Q. Chengrong and L. Zhu, Adsorption Properties of UiO-66/Wood Hybrid Adsorbent for Organic Dye Removal, *Water, Air, Soil Pollut.*, 2023, **234**, 789.

35 Y. Li, L. Rao, L. Hong, P. Si, W. Lin and J. Gao, A modification and selective adsorption of cationic dyes based on UiO-67, *J. Phys. Chem. Solids*, 2024, **184**, 111698.

36 S. A. Younis, A. Abd-Elaziz and A. I. Hashem, Utilization of a pyrrole derivative based antimicrobial functionality impregnated onto CaO/gC 3 N 4 for dyes adsorption, *RSC Adv.*, 2016, **6**, 89367–89379.

37 R. Ediati, L. L. Zulfa, R. D. Putrilia, A. R. P. Hidayat, D. O. Sulistiono, A. Rosyidah, F. Martak and D. Hartanto, Synthesis of UiO-66 with addition of HKUST-1 for enhanced adsorption of RBBR dye, *Arab. J. Chem.*, 2023, **16**, 104637.

38 K. Chinoune, A. Mekki, B. Boukoussa, A. Mokhtar, A. Sardi, M. Hachemaoui, J. Iqbal, I. Ismail, M. Abboud and W. A. Aboneama, Adsorption behavior of MB dye on alginate-sepiolite biocomposite beads: Adsorption, kinetics, and modeling, *Inorg. Chem. Commun.*, 2024, **165**, 112558.

39 S. Tang, D. Xia, Y. Yao, T. Chen, J. Sun, Y. Yin, W. Shen and Y. Peng, Dye adsorption by self-recoverable, adjustable amphiphilic graphene aerogel, *J. Colloid Interface Sci.*, 2019, **554**, 682–691.

40 J. Teresa Jose, K. L. Priya, S. Chellappan, S. Sreelekshmi, A. Remesh, V. Venkidesh, A. J. Krishna, A. Pugazhendhi, S. Selvam, V. Baiju and M. S. Indu, A hybrid electrocoagulation-biocomposite adsorption system for the decolourization of dye wastewater, *Environ. Res.*, 2024, **252**, 118759.

41 Y.-B. Song, X.-D. Song, C.-J. Cheng and Z.-G. Zhao, Poly(4-styrenesulfonic acid-co-maleic acid)-sodium-modified magnetic reduced graphene oxide for enhanced adsorption performance toward cationic dyes, *RSC Adv.*, 2015, **5**, 87030–87042.

42 N. Harsha, K. V. S. Krishna, N. K. Renuka and S. Shukla, Facile synthesis of γ-Fe$_2$O$_3$ nanoparticles integrated H$_2$Ti$_3$O$_7$ nanotubes structure as a magnetically recyclable dye-removal catalyst, *RSC Adv.*, 2015, **5**, 30354–30362.

43 C. Poornachandra, R. M. Jayabalakrishnan, M. Prasanthrajan, G. Balasubramanian, A. Lakshmanan, S. Selvakumar and J. E. John, Cellulose-based hydrogel for adsorptive removal of cationic dyes from aqueous solution: isotherms and kinetics, *RSC Adv.*, 2023, **13**, 4757–4774.

44 Z.-X. Chen, X.-J. Zha, Y.-K. Xia, T.-X. Ling, J. Xiong and J.-G. Huang, 3D Foaming Printing Biomimetic Hierarchically Macro–Micronanoporous Hydrogels for Enhancing Cell Growth and Proliferation, *ACS Appl. Mater. Interfaces*, 2024, **16**, 10813–10821.

45 K. Hu, M. K. Gupta, D. D. Kulkarni and V. V. Tsukruk, Ultra-robust graphene oxide-silk fibroin nanocomposite membranes, *Adv. Mater.*, 2013, **25**, 2301–2307.

46 S. S. Gupta and K. G. Bhattacharyya, Removal of Cd(II) from aqueous solution by kaolinite, montmorillonite and their poly(oxo zirconium) and tetrabutylammonium derivatives, *J. Hazard. Mater.*, 2006, **128**, 247–257.

47 B. H. Hameed, A. L. Ahmad and K. N. A. Latiff, Adsorption of basic dye (methylene blue) onto activated carbon prepared from rattan sawdust, *Dyes Pigm.*, 2007, **75**, 143–149.